



Since January 2020 Elsevier has created a COVID-19 resource centre with free information in English and Mandarin on the novel coronavirus COVID-19. The COVID-19 resource centre is hosted on Elsevier Connect, the company's public news and information website.

Elsevier hereby grants permission to make all its COVID-19-related research that is available on the COVID-19 resource centre - including this research content - immediately available in PubMed Central and other publicly funded repositories, such as the WHO COVID database with rights for unrestricted research re-use and analyses in any form or by any means with acknowledgement of the original source. These permissions are granted for free by Elsevier for as long as the COVID-19 resource centre remains active.

## Structure-based design, synthesis, and biological evaluation of peptidomimetic SARS-CoV 3CLpro inhibitors

Arun K. Ghosh,<sup>a,\*</sup> Kai Xi,<sup>a</sup> Valerie Grum-Tokars,<sup>b</sup> Xiaoming Xu,<sup>a</sup> Kiira Ratia,<sup>b</sup> Wentao Fu,<sup>b</sup> Katherine V. Houser,<sup>c</sup> Susan C. Baker,<sup>c</sup> Michael E. Johnson<sup>b</sup> and Andrew D. Mesecar<sup>b</sup>

<sup>a</sup>Departments of Chemistry and Medicinal Chemistry, Purdue University, West Lafayette, IN 47907, USA

<sup>b</sup>Center for Pharmaceutical Biotechnology and Department of Medicinal Chemistry and Pharmacognosy, University of Illinois at Chicago, 900 S. Ashland, IL 60607, USA

<sup>c</sup>Department of Microbiology and Immunology, Loyola University of Chicago, Stritch School of Medicine, Maywood, IL, USA

Received 28 June 2007; revised 31 July 2007; accepted 1 August 2007

Available online 19 August 2007

**Abstract**—Structure-based design, synthesis, and biological evaluation of a series of peptidomimetic severe acute respiratory syndrome-coronavirus chymotrypsin-like protease inhibitors are described. These inhibitors were designed and synthesized based upon our X-ray crystal structure of inhibitor **1** bound to SARS-CoV 3CLpro. Incorporation of Boc-Ser as the P<sub>4</sub>-ligand resulted in enhanced SARS-CoV 3CLpro inhibitory activity. Structural analysis of the inhibitor-bound X-ray structure revealed high binding affinity toward the enzyme.

© 2007 Elsevier Ltd. All rights reserved.

Severe acute respiratory syndrome (SARS), a contagious and fatal respiratory illness, was first reported in Guangdong province, China, in November 2002.<sup>1</sup> Its rapid and unexpected spread to other Asian countries, North America, and Europe alarmed both the public and the World Health Organization. SARS is caused by a novel coronavirus, SARS-CoV.<sup>2,3</sup> Its emergence affected more than 8000 individuals and caused more than 800 deaths within a few months.<sup>4</sup> This signifies just how rapidly a contagious illness can spread in the more mobile and highly interconnected world in the 21st century. Remarkably, the world has witnessed how concerted international cooperation allowed health experts to identify the novel etiologic agent and contain the SARS epidemic just months after its emergence. Currently, there is no known SARS transmission anywhere in the world. At the same time, there is no guarantee that this outbreak will not strike again in an even more severe form. Thus far, no effective therapy exists for this viral infection.

The SARS-CoV is a positive-strand RNA virus whose genome sequence reveals only moderate relation to other known coronaviruses.<sup>5</sup> During viral replication, viral replicase polyproteins undergo extensive processing by two viral proteases, namely chymotrypsin-like protease (3CLpro) and papain-like protease (PLpro), to generate a functional viral replication complex.<sup>6,7</sup> Therefore, both SARS-CoV 3CLpro and SARS-CoV PLpro are recognized as logical targets for therapeutic intervention against SARS-CoV and related interactions.<sup>8</sup>

The structure and activity of the SARS-CoV 3CLpro have been investigated.<sup>9</sup> The enzyme active site contains a catalytic dyad where a cysteine residue acts as a nucleophile and a histidine residue acts as the general acid base. SARS-CoV 3CLpro is functionally analogous to the main picornaviral protease 3Cpro and there have been significant drug-design efforts against human rhinoviral 3C protease which is also a cysteine protease.<sup>10</sup> We recently described structure-based design of a number of potent SARS-CoV 3CLpro inhibitors.<sup>11</sup> These inhibitors were designed based upon modification of AG7088, a potent inhibitor of the human rhinoviral 3C protease.<sup>12</sup> While AG7088 does not exhibit inhibitory activity against SARS-CoV 3CLpro, the modified

**Keywords:** Design; Synthesis; SARS 3CLpro; Inhibitor; X-ray structure.

\* Corresponding author. Tel.: +1 765 494 5323; fax: +1 765 496 1612; e-mail: [akghosh@purdue.edu](mailto:akghosh@purdue.edu)

inhibitors are active in enzymatic assays as well as in cell culture assays.<sup>13</sup> The X-ray structure of inhibitor-bound SARS-3CLpro revealed important molecular insight into the ligand-binding sites of enzyme.<sup>11</sup> The inhibitors bind to SARS-CoV 3CLpro through covalent bonding with the active site cysteine 145 residue. Based upon this molecular insight, we have now modified our initial inhibitors to accommodate specific ligand-binding site interactions in the S<sub>4</sub>-subsite of the SARS-CoV 3CLpro active site. Herein we describe the synthesis, biological evaluation, and X-ray structures of inhibitor-bound SARS-CoV 3CLpro for two potent peptide and peptidomimetic inhibitors (Fig. 1).

As described previously, inhibitor **2** makes a number of important interactions in the enzyme active site.<sup>11</sup> These include, the covalent bond formed by the Cys-145 thiol with the  $\alpha,\beta$ -unsaturated ester at the S<sub>1</sub>-subsite. His-172 makes hydrogen bond with the P<sub>1</sub>-lactam-NH, and the Glu-166 nitrogen makes a hydrogen bond with the ketone of the inhibitor.<sup>11</sup> The P<sub>4</sub>-oxazole group appears to fill in the S<sub>4</sub>-hydrophobic pocket. Based upon this X-ray structure, we subsequently speculated that the replacement of P<sub>4</sub>-oxazole with a Boc-Serine P<sub>4</sub>-ligand would promote additional hydrogen-bonding interactions in the S<sub>4</sub>-site. This will result in further enhancement of inhibitory potency. We have also evaluated the corresponding peptide-derived inhibitors for our studies.

The synthesis of inhibitor **3** is outlined in Scheme 1. The synthetic procedure of silyl ether derivative **6** was described by us previously.<sup>11</sup> Removal of the silyl protecting group with tetrabutylammonium fluoride in THF provided a secondary alcohol, which was oxidized to ketone **7** with the Dess–Martin periodinane in 73% yield over 2 steps. The ketone **7** was converted to inhibitor **3** by exposure to trifluoroacetic acid (20% TFA/CH<sub>2</sub>Cl<sub>2</sub>)

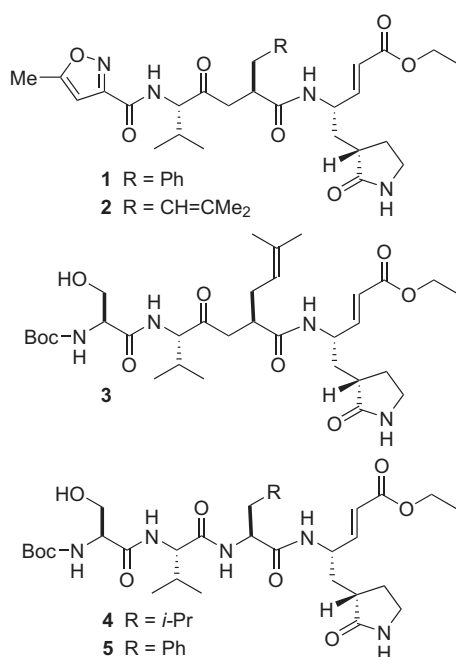
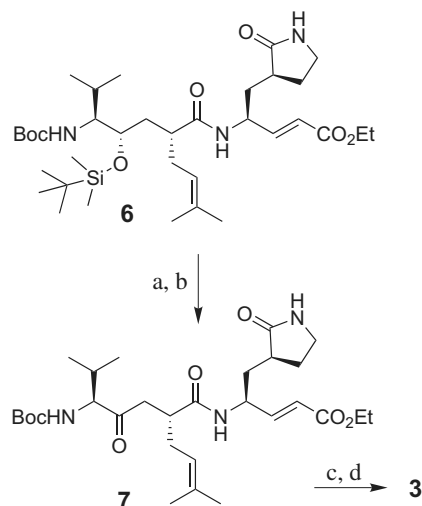


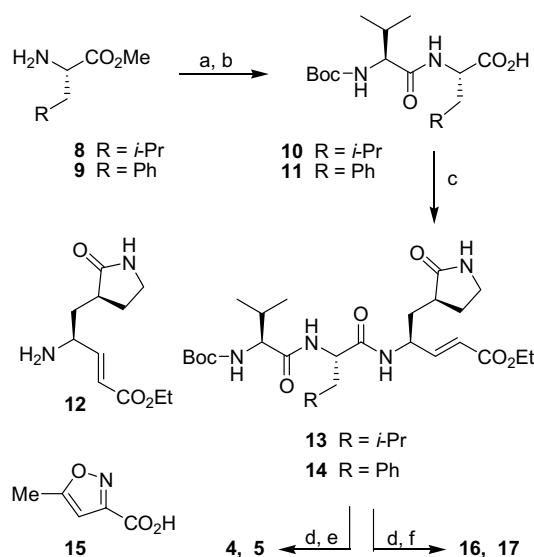
Figure 1. Structures of SARS-3CLpro inhibitors.



**Scheme 1.** Reagents: (a) TBAF, THF; (b) Dess–Martin periodinane, CH<sub>2</sub>Cl<sub>2</sub>, 73% (two steps); (c) TFA, CH<sub>2</sub>Cl<sub>2</sub>; (d) EDC, HOBT, DIPEA, Boc-(L)-Serine, CH<sub>2</sub>Cl<sub>2</sub>, 72%.

followed by coupling of the resulting amine with Boc-(L)-Serine to provide **3** in 72% yield.

The syntheses of peptide-based inhibitors are summarized in Scheme 2. General peptide coupling reactions between (*S*)-valine and (*S*)-leucine or (*S*)-phenylalanine followed by ester hydrolysis gave the carboxylic acid intermediates **10** and **11** in 81% and 90% yields, respectively. Coupling of these acids with lactam fragment **12**<sup>11,14</sup> afforded Boc-derivatives **13** and **14** in 89% and 86% yields, respectively. Exposure of these compounds to TFA effected the removal of the Boc-group to provide the corresponding free amines. Coupling of these amines with Boc-(L)-serine furnished inhibitors **4** and **5** in 55% and 95% yields, respectively. Furthermore, reaction of



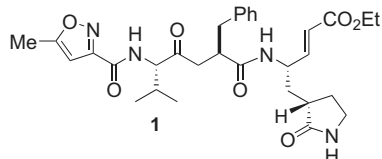
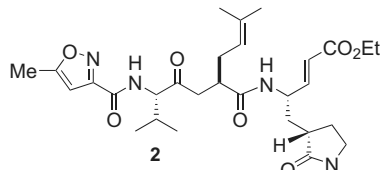
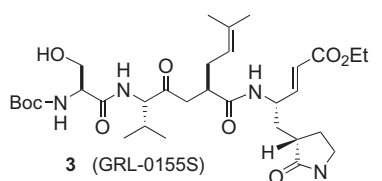
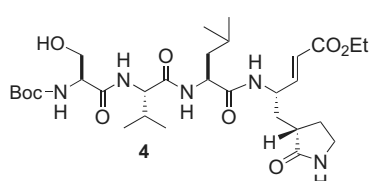
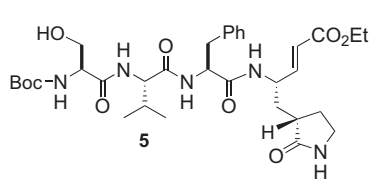
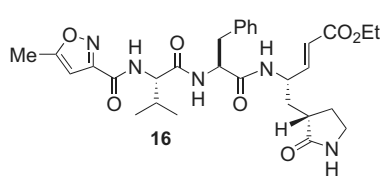
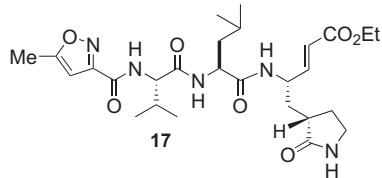
**Scheme 2.** Reagents: (a) EDC, HOBT, DIPEA, Boc-(L)-valine, CH<sub>2</sub>Cl<sub>2</sub>; (b) LiOH (1 M in H<sub>2</sub>O), THF; (c) EDC, HOBT, DIPEA, **12**, CH<sub>2</sub>Cl<sub>2</sub>; (d) TFA, CH<sub>2</sub>Cl<sub>2</sub>; (e) EDC, HOBT, DIPEA, Boc-(L)-Serine, CH<sub>2</sub>Cl<sub>2</sub>; (f) EDC, HOBT, DIPEA, **15**, CH<sub>2</sub>Cl<sub>2</sub>.

the **13** or **14**-derived amines with 5-methylisoxazole-3-carboxylic acid **15**<sup>15</sup> afforded inhibitors **16** (75%) and **17** (81%) in very good yields.

The inhibitory activities of the synthetic inhibitors are shown in Table 1. The enzyme inhibitory activity of the compounds against SARS-CoV 3CLpro was determined in a FRET-based, microplate assay described by Grum-Tokars et al.<sup>11,16</sup> This protocol has previously been used for the determination of IC<sub>50</sub> values for

$\alpha,\beta$ -unsaturated esters.<sup>17</sup> The assays were performed in 96-well microplates using a reaction volume of 100  $\mu$ L which contained 50 mM Hepes, (pH 7.5), 500 nM SARS-CoV 3CLpro enzyme, and varying concentrations of synthetic inhibitors. The reaction components, with the exception of substrate, were incubated for 20 min and the reaction was initiated by the addition of FRET-substrate [AlexaFluor<sup>®</sup> 488-cys]-Glu-Ser-Ala-Thr-Leu-Gln-Ser-Gly-Leu-Ala-[Lys-QSY<sup>®</sup>-7]-Ser, giving a final substrate concentration of 1  $\mu$ M.<sup>11,16</sup> The IC<sub>50</sub>

**Table 1.** Structures and activity of inhibitors

Entry	Inhibitor structure	3CLpro, IC <sub>50</sub> ( $\mu$ M)	Antiviral, IC <sub>50</sub> ( $\mu$ M)
1.		870	45
2.		800	70
3.		80	75
4.		10	100
5.		15	100
6.		300	nd
7.		200	nd

**Table 2.** Summary of X-ray data processing and refinement statistics

Resolution (Å)	$R_{\text{merge}}^b$ (%)	% Complete	$a$ (Å)	$b$ (Å)	$c$ (Å)	$\beta$ (deg)	$R_{\text{cryst}}^c$ (%)	$R_{\text{free}}^d$ (%)	$R_{\text{free}}$ after TLS	$R_{\text{free}}$ after TLS
20.0–1.9 (1.97–1.90) <sup>a</sup>	3.1 (21.7)	91.5 (53.0)	108.32	82.22	53.68	104.67	23.6 (33)	27.5 (36)	19.6 (28)	22.8 (35)

<sup>a</sup> Last shell resolution statistics are shown within parentheses.

<sup>b</sup>  $R_{\text{merge}} = \sum |I - \langle I \rangle| / \sum I$ , where  $I$  is the observed intensity and  $\langle I \rangle$  is the average intensity of multiple symmetry-related observations of that reflection. 118,202 measured reflections. 31,114 unique reflections.

<sup>c</sup>  $R_{\text{cryst}} = \sum ||F_{\text{obs}}| - |F_{\text{calc}}|| / \sum |F_{\text{obs}}|$ , where  $|F_{\text{obs}}|$  and  $|F_{\text{calc}}|$  are the observed and calculated, respectively, structure factor amplitudes for each reflection.

<sup>d</sup>  $R_{\text{free}}$  is the same as  $R_{\text{cryst}}$ , except it is calculated over a set of reflections not used in structural refinement at any stage (5% of the observed data in all cases).

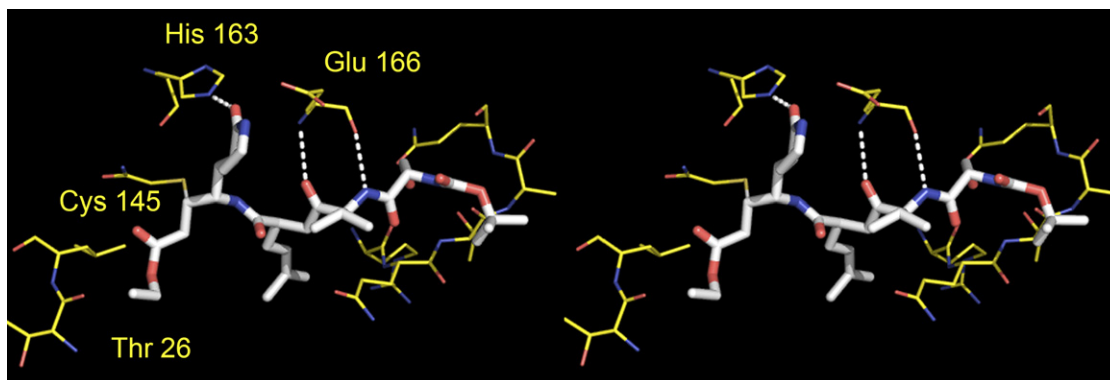


**Figure 2.** The X-ray crystal structure of **3** (thick stick with gray carbon) with SARS-CoV 3CLpro. Hydrogen bonds between inhibitor and 3CLpro are shown in white dotted lines.

values for inhibitors were determined by measuring the rates of reaction with increasing inhibitor concentrations. As shown in Table 1, our structure-based incorporation of P<sub>4</sub>-Boc-Ser in place of P<sub>4</sub>-oxazole in inhibitor **2** resulted in (inhibitor **3**) significant enhancement of enzymatic inhibitory potency, while its antiviral activity was not improved. It exhibited antiviral activity similar to inhibitors **1** and **2**. This difference of activity may be due to the presence of peptide-like features in the inhibitors. Peptide-like molecules often exhibit poor passive transcellular diffusion across cell membranes. Antiviral assays followed our previously published protocol.<sup>11,18</sup> We have compared the binding affinity of the corresponding peptide-based inhibitors incorporating both P<sub>4</sub>-oxazole and P<sub>4</sub>-Boc Ser. Peptide-based inhibitors (**4** and **5**) with P<sub>2</sub>-Leu and P<sub>2</sub>-Phe have displayed 20-fold enzymatic potency enhancement over the respective inhibitors (**16** and **17**) containing P<sub>4</sub>-oxazole.

To obtain molecular insight into the binding properties of inhibitor **3**, we determined the X-ray structure of **3**-bound to SARS-CoV 3CLpro to a resolution of 1.9 Å.<sup>19</sup> The refinement statistics and data collection are summarized in Table 2. A stereoview of the inhibitor-bound structure is shown in Figure 2. The X-ray structure reveals that the inhibitor is covalently bonded to the enzyme via a C–S bond (1.77 Å) to the active site cysteine (Cys-145). The P<sub>1</sub>'-ethyl ester carbonyl is within proximity to Thr-26 oxygen (3.38 Å). The Leu-27 side chain makes hydrophobic contacts with the P<sub>1</sub>'-ligand. Furthermore, the P<sub>1</sub>-lactam NH forms a hydrogen bond with the imidazole ring of His-163. The P<sub>3</sub>-carbonyl group of **3** forms a hydrogen bond with the NH of Glu-166. The P<sub>4</sub>-Ser side chain is within hydrogen-bond-

ing distance of Glu 166. This may explain its enhanced binding affinity over the oxazole-bearing inhibitor **2**.

In conclusion, our structure-based design strategies resulted in significant improvement of enzyme inhibitory activity against SARS-CoV 3CLpro. An X-ray structure of the **3**-bound enzyme provided critical molecular insight into the ligand-binding site interactions in the active site. It appears that the P<sub>4</sub>-Boc-Ser is involved in important hydrogen-bonding interactions in the S<sub>4</sub>'-subsite. The present molecular insight will facilitate the design of more effective inhibitors. Further investigations are in progress.

### Acknowledgment

The financial support of this work is provided by the National Institute of Health (NIAID, P01 A1060915).

### References and notes

- World Health Organization, Communicable Disease Surveillance & Response, website: [http://www.who.int/csr/sars/archive/2003\\_05\\_07a/en](http://www.who.int/csr/sars/archive/2003_05_07a/en) and [http://www.who.int/csr/sars/country/en/country2003\\_08\\_15.pdf](http://www.who.int/csr/sars/country/en/country2003_08_15.pdf).
- Drosten, C.; Gunther, S.; Preiser, W.; van der Werf, S.; Brodt, H. R.; Becker, S.; Rabanau, H.; Panning, M.; Kolesnikova, L.; Fouchier, R. A.; Berger, A.; Burguiere, A. M.; Cinatl, J.; Eickmann, M.; Escouffier, N.; Grywna, K.; Kramme, S.; Manuguerra, J. C.; Muller, S.; Rickerts, V.; Sturmer, M.; Vieth, S.; Klenk, H. D.; Osterhaus, A. D.; Schmitz, H.; Doerr, H. W. *N. Engl. J. Med.* **2003**, *348*, 1967.
- Ksiazek, T. G.; Erdman, D.; Goldsmith, C. S.; Zaki, S. R.; Peret, T.; Emery, S.; Tong, S.; Urbani, C.; Comer, J. A.

- Lim, W.; Rollin, P. E.; Dowell, S. F.; Ling, A. E.; Humphrey, C. D.; Shieh, W. J.; Guarner, J.; Paddock, C. D.; Rota, P.; Fields, B.; DeRisi, J.; Yang, J. Y.; Cox, N.; Hughes, J. M.; LeDuc, J. W.; Bellini, W. J.; Anderson, L. J. *N. Engl. J. Med.* **2003**, *348*, 1953.
4. He, J.-F.; Peng, G.-W.; Min, J.; Yu, D.-W.; Liang, W.-L.; Zhang, S.-Y.; Xu, R.-H.; Zheng, H.-Y.; Wu, X.-W.; Xu, J.; Wang, Z.-H.; Fang, L.; Zhang, X.; Li, H.; Yan, X.-G.; Lu, J.-H.; Hu, Z.-H.; Huang, J.-C.; Wan, Z.-Y.; Hou, J.-L.; Lin, J.-Y.; Song, H.-D.; Wang, S.-Y.; Zhou, X.-J.; Zhang, G.-W.; Gu, B.-W.; Zheng, H.-J.; Zhang, X.-L.; He, M.; Zheng, K.; Wang, B.-F.; Fu, G.; Wang, X.-N.; Chen, S.-J.; Chen, Z.; Hao, P.; Tang, H.; Ren, S.-X.; Zhong, Y.; Guo, Z.-M.; Liu, Q.; Miao, Y.-G.; Kong, X.-Y.; He, W.-Z.; Li, Y.-X.; Wu, C.-I.; Zhao, G.-P.; Chiu, R. W. K.; Chim, S. S. C.; Tong, Y.-K.; Chan, P. K. S.; Tam, J. S.; Lo, Y. M. D. *Science* **2004**, *303*, 1666.
5. (a) Rota, P. A.; Oberste, M. S.; Monroe, S. S.; Nix, W. A.; Campagnoli, R.; Icenogle, J. P.; Peñaranda, S.; Bankamp, B.; Maher, K.; Chen, M.-H.; Tong, S.; Tamin, A.; Lowe, L.; France, M.; DeRisi, J. L.; Chen, Q.; Wang, D.; Erdman, D. D.; Peret, T. C. T.; Burns, C.; Ksiazek, T. G.; Rollin, P. E.; Sanchez, A.; Liffick, S.; Holloway, B.; Limor, J.; McCaustland, K.; Olsen-Rasmussen, M.; Fouchier, R.; Günther, S.; Osterhaus, A. D. M. E.; Drosten, C.; Pallansch, M. A.; Anderson, L. J.; Bellini, W. J. *Science* **2003**, *300*, 1394; (b) Marra, M. A.; Jones, S. J. M.; Astell, C. R.; Holt, R. A.; Brooks-Wilson, A.; Butterfield, Y. S. N.; Khattra, J.; Asano, J. K.; Barber, S. A.; Chan, S. Y.; Cloutier, A.; Coughlin, S. M.; Freeman, G.; Girm, N.; Griffith, O. L.; Leach, S. R.; Mayo, M.; McDonald, H.; Montgomery, S. B.; Pandoh, P. K.; Petrescu, A. S.; Robertson, A. G.; Schein, J. E.; Siddiqui, A.; Smailus, D. E.; Stoot, J. M.; Yang, G. S.; Plummer, F.; Andonov, A.; Artsob, H.; Bastien, N.; Bernard, K.; Booth, T. F.; Bowness, D.; Czub, M.; Drobot, M.; Fernando, L.; Flick, R.; Garbutt, M.; Gray, M.; Grolla, A.; Jones, S.; Feldmann, H.; Meyers, A.; Kabain, A.; Li, Y.; Normand, S.; Stroher, U.; Tipples, G. A.; Tyler, S.; Vogrig, R.; Ward, D.; Watson, B.; Brunham, R. C.; Krajden, M.; Petric, M.; Skowronski, D. M.; Upton, C.; Roper, R. L. *Science* **2003**, *300*, 1399; (c) Ruan, Y. J.; Wei, C. L.; Ee, L. A.; Vega, V. B.; Thoreau, H.; Yun, S. T. S.; Chia, J. M.; Ng, P.; Chiu, K. P.; Lim, L.; Zhang, T.; Chan, K. P.; Oon, L. E. L.; Ng, M. L.; Leo, S. Y.; Ng, L. F. P.; Ren, E. C.; Stanton, L. W.; Long, P. M.; Liu, E. T. *Lancet* **2003**, *361*, 1779.
6. (a) Bartlam, M.; Yang, H.; Rao, Z. *Curr. Opin. Struct. Biol.* **2005**, *15*, 664; (b) Thiel, V.; Ivanov, K. A.; Putics, A.; Hertzog, T.; Schelle, B.; Bayer, S.; Weibrich, B.; Snijder, E. J.; Rabenau, H.; Doerr, H. W.; Gorbalenya, A. E.; Ziebuhr, J. *J. Gen. Virol.* **2003**, *84*, 2305.
7. Ziebuhr, J. *Curr. Top. Microbiol. Immunol.* **2005**, *287*, 57.
8. (a) Chou, K.; Wei, D.; Zhong, W. *Biochem. Biophys. Res. Commun.* **2003**, *308*, 148; (b) Ghosh, A. K.; Xi, K.; Johnson, M. E.; Baker, S. C.; Mesecar, A. D. *Ann. Rep. Med. Chem.* **2006**, *41*, 183.
9. Anand, K.; Ziebuhr, J.; Wadhwani, P.; Mesters, J. R.; Hilgenfeld, R. *Science* **2003**, *300*, 1763.
10. Lawson, M. A.; Semler, B. L. *Curr. Top. Microbiol. Immunol.* **1990**, *161*, 49.
11. Ghosh, A. K.; Xi, K.; Ratia, K.; Santarsiero, B. D.; Fu, W.; Harcourt, B. H.; Rota, P. A.; Baker, S. C.; Johnson, M. E.; Mesecar, A. D. *J. Med. Chem.* **2005**, *48*, 6767.
12. (a) Patick, A. K.; Binford, S. L.; Brothers, M. A.; Jackson, R. L.; Ford, C. E.; Diem, M. D.; Maldonado, F.; Dragovich, P. S.; Zhou, R.; Prins, T. J.; Fuhrman, S. A.; Meador, J. W.; Zalman, L. S.; Matthews, D. A.; Worland, S. T. *Antimicrob. Agents Chemother.* **1999**, *43*, 2444; (b) Matthews, D. A.; Dragovich, P. S.; Webber, S. E.; Fuhrman, S. A.; Patick, A. K.; Zalman, L. S.; Hendrickson, T. F.; Love, R. A.; Prins, T. J.; Marakovits, J. T.; Zhou, R.; Tikhe, J.; Ford, C. E.; Meador, J. W.; Ferre, R. A.; Brown, E. L.; Binford, S. L.; Brothers, M. A.; Delisle, D. M.; Worland, S. T. *Proc. Natl. Acad. Sci. U.S.A.* **1999**, *96*, 11000.
13. Matthews, D. A.; Patick, A. K.; Baker, R. O.; Brothers, M. A.; Dragovich, P. S.; Hartmann, C. J.; Johnson, T. O.; Mucker, E. M.; Reich, S. H.; Rejto, P. A. J.; Rose, P. W.; Zwiers, S. H.; Huggins, J. W. *In Vitro Antiviral Activity of Human Rhinovirus 3C Protease Inhibitors against the SARS Coronavirus*; The National Academies Press: Washington, DC, 2004; Chapter 4, p 186. <http://www.nap.edu/books/0309091543/html/186.htm>.
14. Kokotos, G.; Padron, J. M.; Martin, T.; Gibbons, W. A.; Martin, V. S. J. *Org. Chem.* **1998**, *63*, 3741.
15. Baraldi, P. G.; Simoni, D.; Moroder, F.; Manfredini, S.; Mucchi, L.; Vecchia, F. D. *J. Heterocycl. Chem.* **1982**, *19*, 557.
16. Grum-Tokars, V.; Ratia, K.; Begaye, A.; Baker, S. C.; Mesecar, A. D. *Virus Res.*, in press.
17. Shie, J. J.; Fang, J. M.; Kuo, T. H.; Kuo, C. J.; Liang, P. H.; Huang, H. J.; Wu, Y. T.; Jan, J. T.; Cheng, Y. S.; Wong, C. H. *Bioorg. Med. Chem.* **2005**, *13*, 5240.
18. Antiviral activity was measured against the model coronavirus, mouse hepatitis virus (MHV), using neutral red assay Baker, R. O.; Bray, M.; Higgins, J. W. *Antiviral Res.* **2003**, *57*, 13.
19. The protein–ligand X-ray structure of 3-bound SARS-3 CLpro has been deposited in the Protein Data Bank (PDB code ID: 2QIQ). SARS-CoV 3CLpro was purified using a combination of ion-exchange, ammonium sulfate fractionation, and separation by hydrophobic interaction chromatography according to our published procedures.<sup>16</sup> The refinement statistics and data collection are summarized in Table 2. Purified SARS-CoV 3CLpro was exchanged into buffer (20 mM Tris, pH 7.5, 10% glycerol, and 10 mM 2-mercaptoethanol) and concentrated to 35 mg/mL using an Amicon Centrifugal Filter, molecular weight cutoff 10,000 Da. The enzyme, at a concentration of 35 mg/mL, was incubated with 1 mM inhibitor on ice for 1 h prior to crystallization which was conducted by mixing 5  $\mu$ L enzyme and 1  $\mu$ L of mother liquor solution and allowing the mixture to undergo vapor diffusion against 11% PEG 20,000, 50 mM NaCl, 50 mM Na-cacodylate, pH 6.5. Single crystals grew within 3 h and were cryoprotected and flash-frozen in liquid nitrogen. X-ray data was collected using a MAR-CCD detector at SER-CAT beamline 22-BM at the Advanced Photon Source, Argonne National Laboratory. Data was indexed with HKL2000 and scaled and merged with SCALEPACK (Otwinowski and Minor).<sup>20</sup> The structure was determined via molecular replacement using the coordinates 2ALV from the PDB (Ghosh et al.)<sup>11</sup> and refined with REFMAC from the CCP4 suite (Collaborative, 1994). *R*-Factors were minimized by an additional 4–5% by using 10 cycles of TLS refinement on 19 segments. The 3CLpro-compound 4 complex crystallized in space group C121 with one molecule in the asymmetric unit with unit cell parameters of  $a = 108.32 \text{ \AA}$ ,  $b = 82.22 \text{ \AA}$ ,  $c = 53.68 \text{ \AA}$  and  $\beta = 104.7^\circ$ . The structure was determined by molecular replacement using as a search model. The final  $R_{\text{cryst}}$  and  $R_{\text{free}}$  values were 19.6% and 22.8%, respectively. The final model includes the inhibitor covalently linked to Cys145.
20. Otwinowski, Z.; Minor, W. *Macromol. Crystallogr.* **1997**, *276*, 307.